THE IMPULSIVE X-RAY RESPONSE IN FLARE FOOTPOINTS

T. Mrozek, and M. Tomczak

Astronomical Institute, Wroclaw University, Kopernika 11, PL-51-622 Wroclaw, Poland

ABSTRACT

The impulsive phase of many solar flares well-observed by *Yohkoh* has been investigated using images from the SXT and HXT telescopes. A response to nonthermal electron beams in the individual flare footpoint has been localized and measured. Morphological features such as soft X-ray impulsive brightening and a hard X-ray footpoint emission source have been considered. A correlation between these features has been studied and their dependence on the energy spectrum of nonthermal electron beams has been discussed.

1. INTRODUCTION

The observations of impulsive soft X-ray (SXR) brightenings offer a new diagnostic tool of the nonthermal electrons precipitation in solar flare footpoints. Since the *Yohkoh* discovery of impulsive SXR brightenings (Strong et al. 1994, Hudson et al. 1994) a new method of velocity estimation of the chromospheric evaporation has been developed (Tomczak 1997a). Tomczak (1999) showed that the impulsive SXR brightenings are caused mainly by non-thermal electrons with moderate energies (10-20 keV). He derived also an explanation of the Neupert effect as the result of impulsive SXR brightenings.

In this paper the analysis of Tomczak (1999) was repeated in more comprehensive way for a large number of events.

2. ANALYSIS

For this study we chose flares which impulsive phase were well-observed by *Yohkoh*, their impulsive SXR brightenings were visible after a prompt inspection of the observations and their hard X-ray (HXR) emission in the channels M1 (23-33 keV) and M2 (33-53 keV) had sufficient number of counts for an image reconstruction.

We have investigated the SXT images made with the Al12 filter in which the impulsive SXR brightenings are most evident. The light curves of the individual pixels have been carefully analyzed and those which reached the statistically important maximum of brightness during the impulsive phase were taken into consideration. Neighbouring pixels has been assumed to be a part of the same brightening.

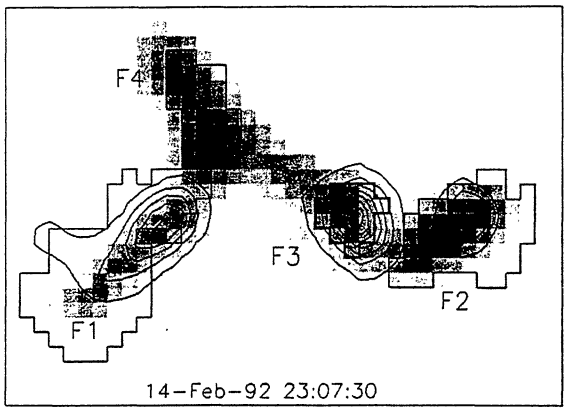

Figure 1. Sample image of the 14-Feb-92 flare obtained at the maximum of the HXR light curve. Grey scale represents the SXT(Al12) emission distribution. The regions of the SXR response, F1, F2, F3 and F4, are marked. Contours of the HXR emmision are overplotted (90, 70, 50, 30 and 10% *of the maximum intensity).*

Every such a brightening was identified to be the footpoint of the flaring magnetic structure. It has been found that usually in these footpoints also HXR emission sources were seen in the images reconstructed using the maximum entropy method (MEM) with new modulation patterns computed by Sato et al. (1999). In Fig. 1 we present an example of the relative position of the SXR brightenings and HXR emission sources in the case of the 14-Feb-92 flare. It should be remarked that there is no visible HXR emission in the footpoint F4. This could be an effect of low dynamic range of the HXT instrument (Sakao 1994).

For the HXR emission sources analysis the time interval near the maximum of the main burst has been

Proc. 10th. European Solar Physics Meeting, 'Solar Variability: From Core to Outer Frontiers', Prague, Czech Republic, 9-14 September 2002 (ESA SP-506, December 2002)

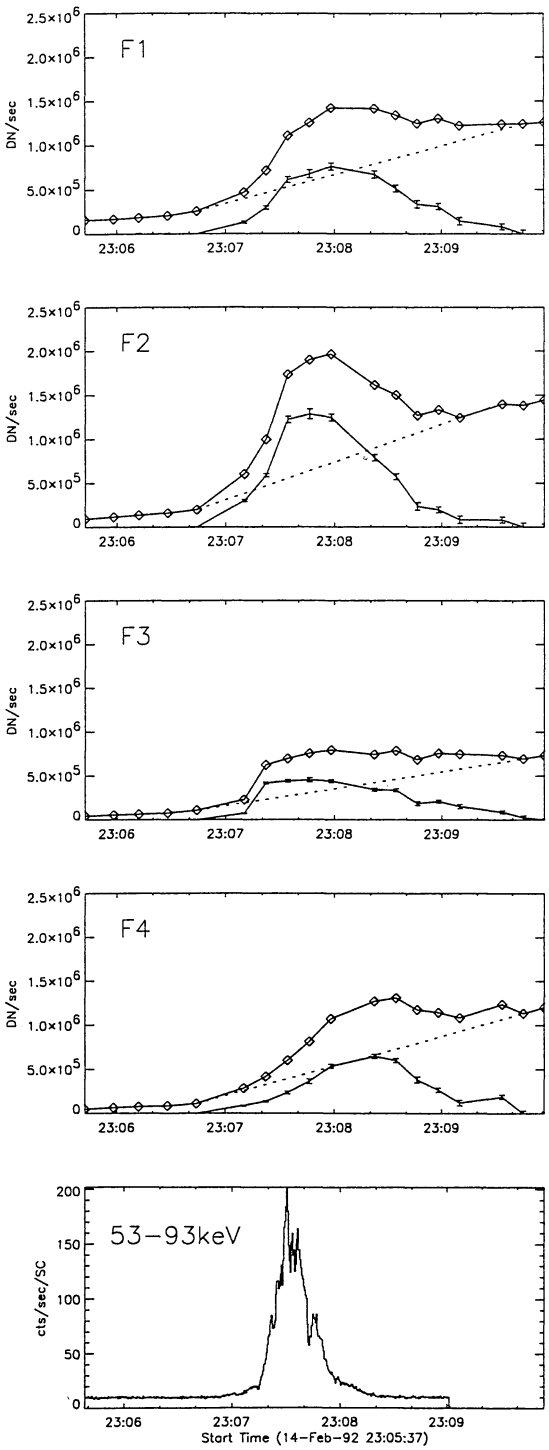

Figure 2. The SXT(Al12) light curves for the footpoints marked in Fig.1. The total as well as the net light curves are presented. The subtracted background is marked by the dotted line. Moreover, the total HTX(H) light curve is showed.

Table 1. List of selected flares

(1)	(2)	(3)	(4)	(5)	(6)
1	$24-Oct-91$	$22:41$	$M9.8$	$1N$	$S12E46$
2	$02-Nov-91$	$06:53$	$X9.0$	$1B$	$S13W61$
3	$10-Nov-91$	$20:13$	$M7.9$	$1N$	$S15E43$
4	$19-Nov-91$	$09:32$	$C8.5$	$1F$	$S12W60$
5	$13-Jan-92$	$17:34$	$M2.0$	–	$S15Wlimb$
6	$26-Jan-92$	$15:33$	$X1.0$	$3B$	$S16W66$
7	$14-Feb-92$	$23:10$	$M7.0$	$2B$	$S13E02$
8	$17-Feb-92$	$15:46$	$M1.9$	SF	$N16W81$
9	$08-Jul-92$	$09:50$	$X1.2$	$1B$	$S11E46$
10	$06-Sep-92$	$09:07$	$M3.3$	$1N$	$S11W38$
11	$16-Jan-94$	$23:25$	$M6.1$	$1B$	$N09E73$
12	$02-Sep-97$	$21:13$	$C4.1$	SF	$N32W41$
13	$14-Sep-97$	$02:55$	$C2.8$	SF	$S23W79$
14	$28-May-98$	$19:12$	$C8.7$	SF	$S20W07$

(1) - Number of event; (2) - Date; (3) - GOES maximum time [UT]; (4) GOES class; (5) - Hα importance; (6) - Coordinates;

chosen. Images synthesized for different channels were compared and the borders of HXR emission were carefully determined.

For further analysis, we selected the impulsive SXR brightenings and the HXR emission sources which showed good spatial correlation (F1, F2 and F3 in the case of the 14-Feb-92 flare) and their light curve peaks showed good temporal correlation (Fig. 2).

Except the impulsive component, caused by non-thermal electron beams, the SXR light curves contain also a long-time, slowly-varying component. We pressumed that this component is caused by other factors, than non-thermal electrons, (e.g. thermal conduction, instrumental factors) and assumed its linear rise in time during the impulsive phase (Tomczak 1999). Such a background was subtracted and net signal, describing a pure SXR response due to non-thermal electrons, has been obtained (Fig. 2).

The HXR photometry was made using images reconstructed with MEM-Sato (Sato et al. 1999) method. We concentrated our attention on the images obtained in higher energy channels (M1, M2 and, H), excepting less thermal contribution.

3. RESULTS

In summary, we found 31 footpoints showing simultaneously the impulsive SXR brightenings and the HXR emission sources. These footpoints come from 14 flares which list is presented in Table 1. Fig. 3 shows a relation between the HXR intensities obtained in the channel M2 and the SXR responses recorded in the Al12 filter. In Fig. 3 also the total

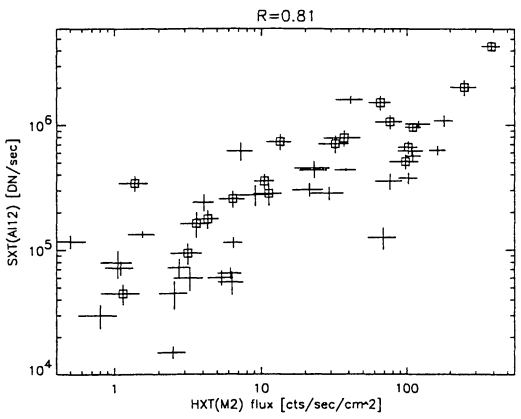

Figure 3. Relation between two kinds of response to the non-thermal electron beams in footpoints observed in HXT(M2) channel and SXT(Al12) filter. R is the correlation coefficient. Total values for the complete events has been marked by squares. See text for further details.

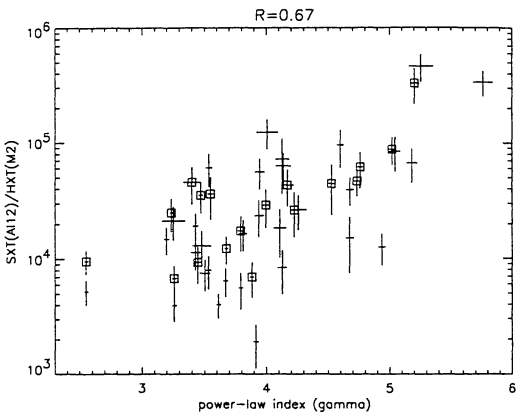

Figure 4. Plot of relative productivity of soft X-rays SXT(Al12) with regard to hard X-rays HXT(M2) and power-law indexes that were taken from single power-law fit. Total values for the complete events has been marked by squares. R is the correlation coefficient. See text for further details.

values for the complete events are presented. For this aim, the peak values of the HXR light curves (no imaging) and the total SXR signal from the all detected brightenings have been used.

The ranges of uncertainties on the both axies were estimated as follows. For SXR the lower limit is the value of the maximum of the net light curve e.g. the light curve with subtracted background. The upper limit is the value of the maximum of the total light curve obtained for the investigated impulsive SXR brightening. For the HXR emission source the lower limit is simply the aggregated flux from all pixels composing footpoint. The upper limit was calculated under the assumption that all faint sources (having intensity below 10 % of the most intense pixel) are produced by any developed reconstruction method (Metcalf et al. 1996, Alexander & Metcalf 1997) and its signal was manually redistributed between the strong sources. These estimated ranges of uncertainties can be considered as a maximal (3σ) error of the SXR response and the HXR emission.

The calculated correlation coefficient, R=0.81, strongly suggests that both observables are the manifestation of a common physical reason, namely non-thermal electron beams. The points representing values for complete events, marked by squares, show better correlation (R=0.91) than those calculated for all values (R=0.81). The main reason of this difference is probably an additional source of errors included by the HXR image reconstruction methods.

There is a scatter, seen in the Fig. 3, which can be caused not only by observational uncertainties and any systematical errors. Points representing individual footpoints of the same event are often situated along a line that is almost perpendicular to the general trend. This effect could be seen in the Fig. 1 where the footpoint F2 seen brighter in SXRs shows the lower HXR emission, while the footpoint F3 shows the opposite relation between those features.

Tomczak (1999) explained this behaviour by comparing values of the power-law index (derived from the hardness ratio M1/M2) for the events showing comparable SXR responses and different HXR intensities. We have repeated this using γ factor obtained from the single power-law fit to the HXR photon fluxes. There is a clear dependence: lower γ is associated with higher HXR intensity.

If we assume that the above relation really exists, then correlation between the relative productivity of SXRs with regard to HXRs and power-law index, also should exist. We divided the mean values of the SXR response by the mean values of the HXR emission for each footpoint. The results are plotted against the power law-index in Fig. 4. The value of the correlation coefficient (R=0.67) is good enough to conclude that the relative productivity of SXR signal with regard to HXR signal rises for higher γ (softer energy spectrum).

Generally speaking, such a relation is a function of the energy of HXR photons. Using values obtained from single power-law fit we calculated photon flux $[photons\, s^{-1}\, cm^{-1}\, keV^{-1}]$ for the each footpoint for several values of the energy. For each value of the energy we calculated correlation between the HXR photon flux and the SXR response. The result is presented in Fig. 5. As we see that the best correlation is for the range 12-15 keV. This is in a good agreement with other observational results (Farnik et al. 1997, Tomczak 1999). Such a value suggests that the impulsive SXR brightenings are caused by relatively low energy electrons.

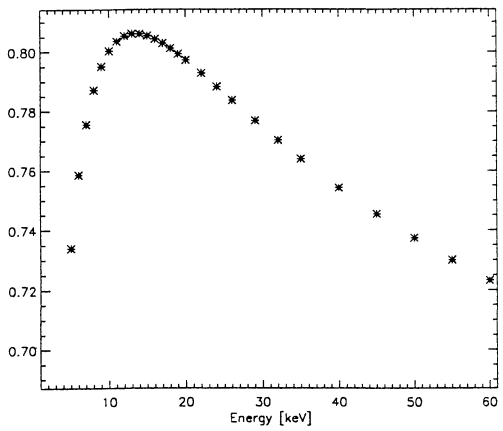

Figure 5. The variability of the correlation between HXR flux [photons s^{-1} cm^{-1} keV^{-1}] and SXR response [DN s^{-1}]. See text for further details.

4. CONCLUSIONS

The *Yohkoh* instruments offer a possibility to investigate impulsive phase using simultaneously the SXR and HXR images. A generally good spatial and temporal correlation between impulsive SXR brightenings and HXR emission sources suggests that they are a manifestation of the same effect, namely non-thermal electron beams. For this reason the SXT images are complementary with the HXT images in the monitoring of the non-thermal electron precipitation during the flare impulsive phase. The role of the SXT in such an ivestigation is very important because this instrument offers better spatial resolution and dynamical range than the HXT. Moreover, there is no spurious sources in the SXR images.

For large number of events we compared the impulsive response in flare footpoints observed in the SXR and the HXR images. There is a clear relationship between these parameters which allows to expect the common physical origin, namely non-thermal electron beams (Tomczak 1999).

However, there is some evidences, for example the scatter in Fig. 3, suggesting a more complicated relationship between the ivestigated observables. It has been found that a stepper energy spectrum of HXR photons causes a higher SXR productivity (Tomczak 1999). We showed for greater number of events that this correlation is still evident. This means that the previous result, obtained by Tomczak (1999), was correct in spite of a small number of the investigated events.

We found that the SXR brightenings are caused by relatively low-energy electrons. More energetic electrons should reach the denser atmospheric layers (Farnik et al. 1997) and produce an impulsive reaction seen in the UV radiation. Such a scenario may be examined by using simultaneously the *Yohkoh*, the *SOHO/EIT* and the *TRACE* images.

It can be seen (Fig. 2) that footpoints show response to non-thermal electrons but they react in different moments of time. Such an effect can be explained by the turbulent kernel model (Jakimiec et al. 1998). In this model non-thermal electrons are able to escape outside the turbulent kernel only during reconnection with external magnetic lines of force. If the external lines are rooted somewhere in the chromosphere we observe there the SXR and HXR response.

ACKNOWLEDGEMENTS

The *Yohkoh* satellite is a project of the Institute of Space and Astronautical Science of Japan. This investigation has been supported by grant No. 2 P03D 001 23 from the Polish Committee for Scientific Research (KBN).

REFERENCES

Alexander, D., & Metcalf, T.R. 1997, ApJ, 489, 442

Farnik, F., Hudson, H., & Watanabe, T. 1997, A&A, 320, 620

Hudson, H., Strong, K., Dennis, B., Zarro, D., Inda, M., Kosugi, T., & Sakao, T. 1994, ApJ, 422, L25

Jakimiec, J.,Tomczak, M., Falewicz, R.,Phillips, K.J.H., & Fludra, A. 1998, A&A, 334, 1112

Metcalf, T,R., Hudson, H.S., Kosugi, T., Puetter, R.C., & Piña, R.K. 1996, ApJ, 466, 585

Sakao T. 1994, Ph.D. Thesis, University of Tokyo

Sato, J., Kosugi, T., & Makishima, K. 1999, Publ. Astron. Soc. Japan, 51, 127

Strong, K., Hudson, H., & Dennis, B., X-Ray Solar Physics from *Yohkoh*, ed. Y. Uchida, T. Watanabe, K. Shibata, & H.S. Hudson 1994, Universal Academy Press (Tokyo), pp. 65

Tomczak, M. 1997, A&A, 317, 223

Tomczak, M. 1999, A&A, 342, 583